Development of a fs/ps CARS system for temperature measurements in supersonic and hypersonic environments

Anna L. Stevenson*, Chloe E. Dedic†
University of Virginia, Charlottesville, VA 22903

Neil S. Rodrigues‡, Paul M. Danehy§
NASA Langley Research Center, Hampton, Virginia, 23681

A hybrid femtosecond/picosecond coherent anti-Stokes Raman scattering (fs/ps CARS) system was developed for quantitative measurements of temperature in a laboratory-scale supersonic jet facility. Measurements were recorded at low pressures and densities relevant for supersonic and hypersonic environments, with special interest in exploring the feasibility of deploying this technique in the 20-inch Mach 6 and 31-inch Mach 10 wind tunnels located at NASA Langley Research Center. Modifications to the existing supersonic jet facility were made to simulate a test section with a width of 31 inches, so that the size of the test section is relevant for either wind tunnel. The CARS system was designed such that a similar beam geometry can be used in the laboratory to acquire point-based fs/ps CARS measurements along two axes of translation. Rotational Raman transitions of O_2 and N_2 were targeted.

I. Introduction

The development of hypersonic vehicles requires a comprehensive understanding of the gas flow around the vehicle. Hypersonic flow fields over a body have distinct characteristics from other supersonic flow fields, including (a) high prevailing temperatures in the post-shock gases resulting in a highly reactive environment, (b) short residence times of gas molecules around the flight system, (c) high rates of aerodynamic heating of the fuselage, and (d) the absence of linearity in the inviscid slender-body limit [1]. Thorough understanding of hypersonic flows is critical as it can impact the design of hypersonic vehicles and subsystems, including the thermal protection and flight control systems [2]. Computational fluid dynamics (CFD) simulations may be used to characterize these flowfields, though there are many complex phenomena for which CFD is inaccurate as these simulations rely on models which make thermal, mathematical, and/or chemical assumptions about the flowfield [3]. Additionally, some flight conditions or test configurations lack suitable experiments or measurement methodology to provide relevant data for CFD validation. Thus, experimentation with accurate, in-situ measurement systems is needed to validate CFD simulations and ensure flowfields are accurately characterized.

Hypersonic wind tunnels are the primary research approach for high temperature gas dynamics, and well-designed experiments can yield reliable data. The measurement technologies used to study these flows can broadly be broken down into three categories: heat-transfer measurements, aerodynamic balance, and optical diagnostics [4]. Both heat-transfer measurements and aerodynamic balance are invasive studies, where a sensor (i.e., calorimeter, surface thermometer, strain gauge) is placed in the tunnel and/or on a model to collect data. These measurement techniques are limited by sensor life and their accuracy may be affected by sensor oxidation (due to the highly reactive environment) and the high temperature environment [5, 6]. In-situ based optical diagnostics can improve measurement accuracy, as well as allow for multi-parameter detection of thermodynamic properties (i.e., temperature, pressure, and species concentration), off-body measurements with spatial precision, and increased time resolution [7].

Optical diagnostic techniques including planar laser induced fluorescence [8, 9], schlieren imaging [10, 11], Rayleigh scattering [12, 13], molecular tagging velocimetry [14], focused laser differential interferometry [9], and coherent Raman scattering [15, 16] have been used to study hypersonic flows. In particular, Raman spectroscopy has been proven to provide reliable information about rotational and vibrational temperatures, and it offers chemical selectivity as energy level spacing differs between molecules. Coherent anti-Stokes Raman scattering (CARS) offers excellent signal strength,

*Graduate Research Assistant, Department of Mechanical and Aerospace Engineering, AIAA Student Member
†Assistant Professor, Department of Mechanical and Aerospace Engineering, AIAA Senior Member
‡Optical Physicist, Advanced Measurements and Data Systems Branch, AIAA Member
§Senior Technologist, Advanced Measurements and Data Systems Branch, AIAA Associate Fellow

shortened acquisition time, and improved background suppression when compared to other forms of Raman scattering [7]. CARS also offers improved spatial resolution over optical diagnostic techniques typically deployed in large-scale facilities. Additionally, as CARS is a spatially resolved 0D or 1D measurement, temperatures may be quantified at a number of locations where a thermocouple may not be easily accessible, allowing for increased understanding of the flowfield in a non-invasive manner. However, the use of CARS in low pressure environments is difficult due to the dependence of the CARS signal on the number density squared of gas molecules [17]. Additionally, the implementation of CARS in wind tunnel facilities is difficult as complex optical setups are required in a facility which may have limited access and run times [17].

This work aims to study the feasibility of deploying fs/ps CARS to measure gas temperature in supersonic and hypersonic wind tunnels, notably the 20-inch Mach 6 and 31-inch Mach 10 air wind tunnels at NASA Langley Research Center. A laboratory-scale supersonic jet facility with window extensions (to provide a cross-section relevant to both wind tunnels) was used to develop and test the optical system. Testing occurred at a variety of pressures and densities relevant to supersonic and hypersonic environments. Translation stages were used to collect temperature measurements in two directions, parallel and perpendicular to the direction of laser propagation.

II. Hybrid fs/ps CARS Theory

Hybrid fs/ps CARS is a nonlinear, four-wave mixing process that utilizes two fs pulses and one ps pulse overlapped spatially and temporally to produce a coherent laser-like signal containing thermodynamic information about the gas sample. Hybrid fs/ps CARS combines the broadband excitation of a femtosecond laser with narrowband picosecond detection, which allows for the suppression of nonresonant background and increases the accuracy of the CARS measurement when the exact collisional environment is not known. The two fs pulses (ω_{pump}, ω_{Stokes}) are used to excite vibrational or rotational molecular transitions, and the ps probe (ω_{probe}) is used to probe the molecular response. The generated CARS signal (ω_{CARS}) can provide information about the temperature, pressure, and species concentrations of the molecules in the probe volume [18]. Frequency and timing diagrams for pure rotational S-branch hybrid fs/ps CARS are shown in Fig. 1. For this experiment, rotational transitions of O_2 and N_2 will be targeted using the frequency difference between ω_{pump} and ω_{Stokes}.

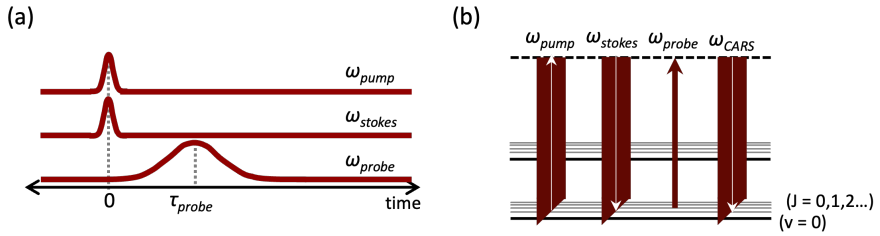

Fig. 1 (a) Timing and (b) frequency diagrams for pure-rotational S-branch fs/ps CARS.

The interaction of the pump, Stokes, and probe pulses result in a third-order polarization field. The CARS intensity $I_{CARS}(\omega)$ is proportional to the resonant and nonresonant third-order polarizations, $P^{(3)}_{res}(\omega)$ and $P^{(3)}_{nonres}(\omega)$, respectively:

$$I_{CARS}(\omega) \propto |P^{(3)}_{res}(\omega) + P^{(3)}_{nonres}(\omega)|^2 \tag{1}$$

The nonresonant polarization can be neglected by delaying the probe pulse in time relative to the initial excitation. The resonant polarization can be expressed as

$$P^{(3)}_{res}(\omega) = (i/\hbar)^3 E_3(t) \int_0^\infty dt_2 [R_4(t_2) E_2^*(t + \tau_{23} - t_2) E_1(t + \tau_{23} + \tau_{12} - t_2) exp[i(\omega_1 - \omega_2)]] \tag{2}$$

where E_1, E_2, and E_3 refer to the electric fields of pump, Stokes, and probe, respectively. τ_{12} refers to the delay between pump and Stokes (which is equal to 0), and τ_{23} refers to the delay between probe and Stokes [19]. For well-separated Raman transitions, the molecular response R_4 is expressed as

$$R_4(t) = \sum_{i,f} (\frac{d\sigma}{d\Omega} \Delta p(T))_{i,f} exp[-(i\omega_{i,f} + \Gamma_{i,f})t] \tag{3}$$

where i and f denote the initial and final quantum states, respectively, c is the speed of light, $\omega_{i,f}$ is the transition frequency, $\Gamma_{i,f}$ is the total Raman linewidth including Doppler and collisional broadening, $d\sigma/d\Omega$ is the Raman cross section, and $\Delta p(T)$ is the temperature-sensitive population difference between relevant states as described by the Boltzmann distribution [20]. The change in energy level is dictated by selection rules for pure-rotational S-branch Raman transitions (Δv = 0, ΔJ = +2). These general equations are used to simulate CARS spectra, which can be compared against experimentally acquired CARS spectra to extract thermodynamic properties such as temperature. The fitting routine is described in more detail in [21]. Briefly, a library of CARS spectra at a variety of temperatures is generated; experimental parameters such as probe bandwidth, time delay, and pump and Stokes bandwidth are included in modeling the spectral library. Each experimental spectrum is then compared to the simulation library using a differential evolutionary algorithm to determine the experimental temperature.

The spatial resolution of CARS is dictated by the spatial extent over which the three laser beams are overlapped, phase matching is satisfied, and the electric field intensity is sufficient. Phase matching satisfies the conservation of momentum:

$$\vec{k}_{pump} - \vec{k}_{Stokes} + \vec{k}_{probe} = \vec{k}_{CARS} \tag{4}$$

Here, $\vec{k}_i$ refers to the wavevector corresponding to the frequency ω_i. Phase matching can be accomplished through a variety of beam crossing configurations; a folded BOXCARS configuration was employed in this experiment [22]. Proper phase matching enables maximum CARS signal generation, and the folded BOXCARS configuration enables spatial discrimination of the CARS signal from the pump, Stokes, and probe beams [23].

III. Background: 20-inch Mach 6 and 31-inch Mach 10 wind tunnels

This work aims to study the feasibility of deploying CARS in supersonic and hypersonic environments for temperature measurements. The target facilities are the 20-inch Mach 6 and 31-inch Mach 10 wind tunnels located at NASA Langley Research Center in Hampton, Virginia, USA. The Mach 6 tunnel is a perfect-gas, blowdown facility with a nominal Mach number of 6 and a 20.5-inch by 20-inch test section. The system is described in depth in [3] and is summarized here. The working fluid is dried, filtered air. The tunnel is capable of producing freestream Reynolds numbers from $0.5x10^6$/ft to $8.0x10^6$/ft. The test section, shown in Figure 2a, is optically accessible through windows on the top and sides. Freestream temperature, stagnation pressure, and number density for three nominal conditions are located in Table 1. Number density is reported in amagats, where an amagat is defined as the number of ideal gas molecules per unit volume at 1 atm and 0 °C. The number density (in amagats) of a gas at pressure p and temperature T can be calculated using $n = \frac{p}{p_0}\frac{T_0}{T}$, where T_0 = 273.15 K and p_0 = 101.325 kPa.

The Mach 10 tunnel is an electrically-heated blowdown facility with a nominal Mach number of 10 and a 31-inch square test section. The system is described in depth in [3] and [24] and is summarized here. The working fluid is dried, filtered air. Air flows from the high pressure heating section through the settling chamber, a three-dimensional water-cooled contoured nozzle, the test section, second minimum, aftercooler, and then into vacuum spheres that are evacuated by steam ejectors and vacuum pumps. The test section, shown in Fig. 2b, is optically accessible through windows on three walls (top, bottom, and one side). The tunnel is capable of producing freestream Reynolds numbers from $0.25x10^6$/ft to $2.2x10^6$/ft. Freestream temperature, stagnation pressure, and number density (in amagats) for three nominal conditions are located in Table 2.

Table 1 Nominal test conditions for the 20-inch Mach 6 wind tunnel.

T (K)	P_0 (Torr)	Number Density n (amg.)
60	1.9	0.012
63	12.0	0.068
59	15.5	0.095

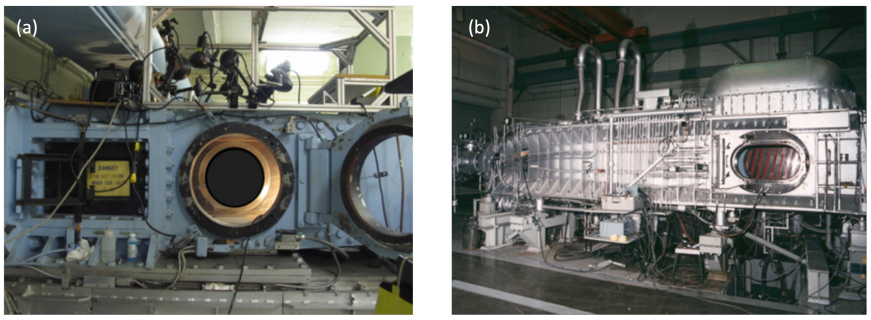

Fig. 2 NASA Langley Research Center (a) Mach 6 and (b) Mach 10 air tunnels [3].

Table 2 Nominal test conditions for the 31-inch Mach 10 wind tunnel.

T (K)	P_0 (Torr)	Number Density n (amg.)
51.6	0.5	0.0035
50.4	1.0	0.0071
49.5	1.7	0.012

IV. Experimental Setup

The fs/ps CARS optical system was tested using a laboratory-scale supersonic jet facility described in Section IV.A as a proof of concept for eventual use in the Mach 6 and Mach 10 tunnels. Optical access in the Mach 10 tunnel requires that the beams propagate vertically through the top and bottom window, perpendicular to the direction of flow. Optical access in the Mach 6 tunnel requires that the beams propagate horizontally through the two side windows, which are also perpendicular to the direction of flow. The experimental CARS system employed in this study allows for axial translation in two dimensions; a straightforward upgrade would allow for translation in the third axis upon installation within a large-scale tunnel. The directions of translation implemented in the laboratory-scale supersonic jet facility allow for the probe volume to be centered in the flow path and for temperature measurements to be collected at a variety of locations from the centerline of the flow to the side windows.

A. Supersonic flow facility

The test facility used to develop and test the CARS system is a laboratory-scale supersonic flow facility designed to match supersonic and hypersonic tunnel conditions. The facility is described in detail in [20] and summarized here. The flow system consists of a high pressure air supply, a mass flow controller, a supersonic flow nozzle with a plenum, and a vacuum chamber system. A vacuum pump was used to operate the supersonic nozzles in a nearly perfectly expanded or pressure-matched condition. A pressure gauge and thermocouple are used to monitor the total pressure and temperature of the supersonic nozzle plenum; a separate pressure gauge is used to monitor the vacuum chamber pressure. The vacuum chamber test section, containing the exit of the supersonic nozzle, is optically accessible on four sides. Vacuum fittings were added to two sides of the test section such that its width—in the direction of beam propagation—was 31 inches. The facility is capable of running a pressure-matched jet, as shown in Fig. 3. Pressure-matched conditions result in a uniform volume of constant-property fluid at the exit of the nozzle, which last for approximately 1 nozzle diameter downstream. Therefore, the test conditions for the experiment are well known, which enables studying the accuracy of temperature measurements acquired using CARS in different environment.

CARS signal was acquired in a pressure-matched jet created using interchangeable nozzles with nominal Mach numbers of 1.8, 2.7, and 4.0. Previous experiments determined, using a pitot probe, that the average Mach numbers correspond to M =1.84, 2.64, and 3.84, respectively [20]. The static temperature (T_s) and pressure (p_s) at the exit of the nozzles were varied by changing the nozzle to vary the Mach number, and by adjusting stagnation pressure (p_t) while maintaining a stagnation temperature (T_t) of 296 K. T_s and p_s can be calculated by assuming an adiabatic, isentropic flow:

$$p_s = p_t \left(1 + \frac{(\gamma - 1)}{2} M^2\right)^{-\gamma/(\gamma-1)} \tag{5}$$

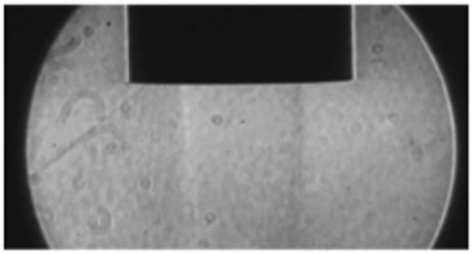

Fig. 3 Schlieren image of a Mach 1 jet, demonstrating the facility running a pressure-matched jet [20].

$$T_s = T_t \left(1 + \frac{(\gamma - 1)}{2} M^2\right)^{-1} \tag{6}$$

A constant value of 1.4 was used for the ratio of specific heats (γ). The experimentally determined Mach numbers from [20] were used for M. The three supersonic nozzles used for CARS measurements and their exit jet conditions are included in Table 3. The exit diameters of the Mach 1.84, 2.64, and 3.84 nozzles are 9.96 mm, 7.47 mm, and 5.44 mm, respectively. CARS measurements were acquired at a single exit condition for the Mach 1.84 and 2.64 nozzles, and at three different exit conditions for the Mach 3.84 nozzle. Additionally, CARS measurements were acquired in a static vacuum cell, where pressure was varied from 7 to 760 torr, and temperature remained constant at 296 K.

Table 3 Static pressure and temperature conditions for three supersonic nozzles studied using the laboratory-scale supersonic jet facility.

M	T_s(K)	P_s (Torr)	Number Density n (amg.)
1.84	175	135	0.299
2.64	122	135	0.398
3.84	74	42	0.220
3.84	74	24	0.125
3.84	74	13	0.068

The CARS setup was designed as a proof of concept for the Mach 6 and Mach 10 tunnels, where the translation directions of interest are used to center the probe volume in the direction of flow and enable transverse translation from the center of the flow to the sidewall, as shown in Fig. 4. Translation stages were implemented in a similar configuration in the laboratory-scale supersonic jet facility, with the individual stages translating perpendicular to and parallel to the direction of flow. One translation stage, labelled TS1 in Fig. 4, simulates the transverse translation required in the Mach 6 and Mach 10 tunnels to acquire measurements from the centerline of the flow to the side wall. The other translation stage, labelled TS2, allows for the probe volume to be centered on the jet in the direction of beam propagation. For both Mach 6 and Mach 10 tunnels, the corresponding translation stage would enable centering the probe volume in the test section, but the stage will now move parallel to instead of perpendicular to the flow. Details regarding the optics to be translated are provided in Section IV.B.

B. fs/ps CARS

The experimental fs/ps CARS setup is shown in Fig. 5. The fs/ps CARS system for the current work is modified from [20], where more experimental details are outlined. Briefly, a laser cart includes a 1-kHz, regeneratively-amplified, 70-fs Ti:sapphire laser (Solstice, Spectra Physics), pulse-shaping optics, and optical delay stages. The output of the Solstice is directed to a waveplate and thin film polarizer. A portion of the beam (0.25 mJ) is used to form the pump/Stokes pulse, represented in Fig. 5 as a black line. The remaining energy is directed into a $4f$ pulse shaper, consisting of a grating (1500 lpmm), a cylindrical lens ($f = 300\,mm$), and a mirror assembly with a slit. The cylindrical lens is placed $1f$ from the face of the grating, and the face of the mirror is placed $1f$ from the cylindrical lens. The output of the $4f$ pulse shaper is the probe pulse, now on the order of picoseconds. The probe pulse duration was measured by flowing a jet of

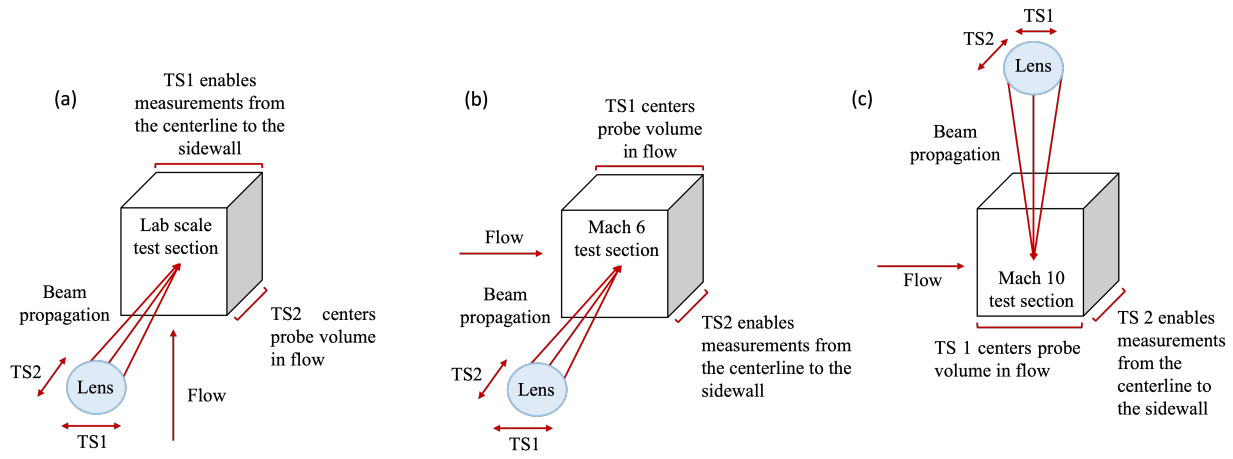

Fig. 4 Orientation of the test section, flow path, beam propagation, and translation stages for (a) the laboratory-scale supersonic jet facility, (b) the Mach 6 wind tunnel, and (c) the Mach 10 wind tunnel. Translation stages controlled the movement of the optics, allowing CARS measurements to be acquired at multiple locations.

nonresonant gas (argon) and cross-correlating the ps probe pulse with the fs excitation pulses. The measured duration was 7 ps. Previously, a similar optical setup (with a double slit in place of a single slit) was used to acquire temperature and pressure measurements at the exit of a supersonic nozzle using a two-probe technique [20]. Although pressure measurements are outside the scope of this paper, the infrastructure for a second probe pulse remains, should pressure measurements be desired in future test campaigns. In this experiment, a motorized stage allowing for up to 1000 ps of total travel is used to control probe delay for temperature measurements.

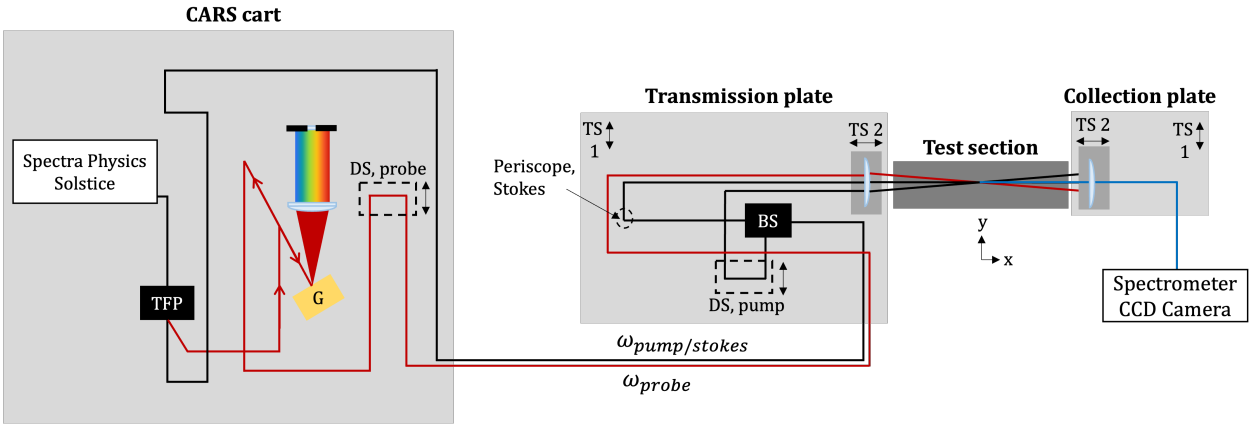

Fig. 5 Optical arrangement for fs/ps CARS experiments. The CARS cart housing the fs amplifier (Solstice), pulse-shaping optics, and optical delay lines (G: grating, TFP: thin film polarizer, DS: delay stage) contains mirrors at the cart exit which direct the pump/Stokes (black line) and probe (red line) beams to the transmission plate. The transmission and collection plates are shown oriented around the test section (BS: beam splitter, TS: translation stage).

Mirrors at the edge of the cart are used to direct the two beams—pump/Stokes (Δt = 70 fs, λ = 800 nm) and probe (Δt = 7 ps, λ = 800 nm)—to an optical plate, referred to as the transmission plate, adjacent to the test section. This transmission plate is placed on a motorized translation stage (TS 1), which allows for the translation of the probe volume radially across the jet, from the centerline to the sidewall. On this stage several mirrors are used to direct the beams to the probe volume; a beam splitter is used to separate the combined pump/Stokes beam. The Stokes beam is directed to a higher plane using a periscope to achieve the folded BOXCARS phase-matching orientation. The three beams are directed onto a 750-mm focal length lens; this focal length was chosen to simulate the focusing conditions

required for taking CARS measurements in either the 20-inch Mach 6 or 31-inch Mach 10 tunnels. The lens is placed on an additional motorized translation stage, labelled TS 2, which allows for the probe volume to be centered on the nozzle exit. The beams are then focused in a folded BOXCARS configuration (crossing angle 1.15°) and overlapped in the measurement region, or probe volume, in the test section. The probe volume, measured using a glass slip, was determined to be 7.8 mm at the full-width 10%-maximum and was at a height of 2 mm above the exit of the jet. After crossing in the test section the beams and generated CARS signal, shown in Fig. 5 in blue, pass through a second 750 mm focal length lens to collimate the CARS signal. The folded BOXCARS configuration allows for sufficient spatial separation of the four beams at the collection lens. After the collection lens all beams except for the CARS signal were terminated and the CARS signal routed to a 0.3-m spectrometer (Andor Kymera 328i) and EMCCD camera (Princeton Instruments PhotonMax, 70% quantum efficiency at 800 nm). The full camera chip (512x512 pixels) was binned vertically. A third motorized translation stage, which moved in conjunction with TS 1, was used to adjust the lens on the collection plate. A fourth motorized translation stage, which moved in conjunction with TS2, was used to adjust the the lens and turning mirrors used to route CARS signal to the spectrometer. To enable single shot detection, the fs laser and EMCCD camera were synchronized and operated at 200 Hz (the maximum frame rate of the EMCCD camera).

V. Results

A. Static gas measurements

CARS measurements were recorded in a static air environment at 296 K, and the vacuum chamber pressure was varied from 760 torr (1 atm) to 7 torr. CARS signal was collected using the spectrometer and EMCCD and binned vertically; 1000 single-shot spectra were acquired at each test condition. A measured temperature was determined for each single-shot spectrum; an average temperature and standard deviation in temperature was then calculated. Additionally, the individual single-shot spectrum were averaged together and then compared against the library of spectra to determine an ensemble average temperature. All spectra were background subtracted and normalized before averaging. A linear baseline correction was used to account for degenerate light scattering at a Raman shift of 0 cm^{-1}.

Sample temperature fits for single-shot spectra at vacuum pressures of 760 torr, 135 torr, and 76 torr are shown in Figure 6. Histograms showing the distribution of temperature fits at these conditions are shown in Figure 7; the average fit temperature at each condition is plotted as a vertical line. The average measured temperatures at vacuum pressures of 760 torr, 135 torr, and 76 torr were 294 K, 291 K, and 286 K, respectively. These values correspond to measurement inaccuracies of 2.2%, 3.5%, and 6.1%. Ensemble averaged temperature fits for 760 torr, 135 torr, and 76 torr are shown in Figure 8. The ensemble average measured temperatures at vacuum pressures of 760 torr, 135 torr, and 76 torr were 294 K, 293 K, and 289 K, respectively. In Figures 6 and 8, the experimental spectra are plotted as red symbols, the best-fit library spectra are shown as a black curve, and the difference between the two is shown offset as blue symbols. It can be seen in Figure 6 that as vacuum pressure decreases and, consequently, number density decreases (as temperature remains constant), the noise in the CARS spectra increases. Increased noise in the CARS spectra leads to increased difficulty when using the temperature fitting routine, which can result in increased error. Specifically for rotational CARS spectra, which have a large number of spectral features available for temperature fitting when compared with rovibrational fs/ps CARS, the temperature-sensitive features at high wavenumber can become masked in noise. This can result in a fitting routine converging on a temperature that is lower than reality; such is the case for the 76 torr condition, where the average fit temperature is 286 K–10 K lower than expected. The increased error in the fitting routine as number density decreases is also apparent in Figure 7; as the vacuum pressure decreases, the distribution of fit temperature broadens. The histograms for the 135 torr and 76 torr conditions are both skewed toward temperatures lower than 296 K. Ensemble averaging the spectra can assist in minimizing the impact of increased single-shot noise, as can be seen in Figure 8. After ensemble averaging, there is negligible increase in the noise at 135 torr and 76 torr compared to 760 torr. Additionally, the ensemble average temperatures–294 K (760 torr), 293 K (135 torr), and 289 K (76 torr)–are in good agreement with one another and the expected temperature at these three conditions.

CARS measurements were acquired at 10 different vacuum pressures varying from 7 torr to 760 torr. The average temperature and standard deviation in temperature from fitting each single-shot spectrum are shown in Figure 9, where the blue markers denote average temperature and the error bars denote standard deviation. Ensemble average temperature is also shown in Figure 9, denoted with a red triangle marker. Additionally, the signal-to-noise ratio (SNR) at each pressure is denoted with a black diamond marker. SNR is discussed in more depth in Section V.C; briefly, SNR is defined as the average peak CARS signal divided by the standard deviation of the noise (this metric neglects shot noise). It can be seen that up until a vacuum pressure of 135 torr, the single-shot average and ensemble average temperature

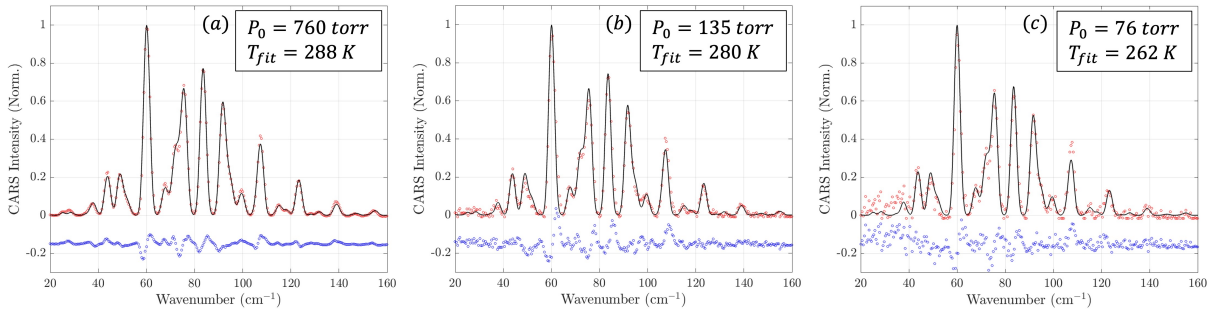

Fig. 6 Single-shot temperature fits of CARS spectra of air acquired in a static cell at 296 K and a vacuum pressure of (a) 760 torr, (b) 135 torr, and (c) 76 torr. Increased noise can be seen in the residuals of the temperature fit at 135 torr when compared against the residuals for the temperature fit at 760 torr; a significant increase in noise is visible in the residuals of the temperature fit at 76 torr. Increased noise in the spectra results in the fitting routine converging at a lower temperature than expected.

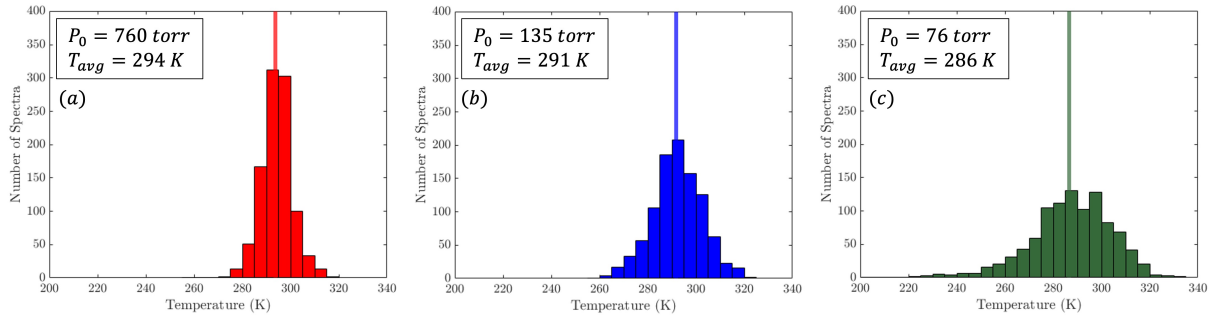

Fig. 7 Histograms of single-shot temperature fits of CARS spectra of air acquired in a static cell at 296 K and a vacuum pressure of (a) 760 torr, (b) 135 torr, and (c) 76 torr. As the vacuum pressure (and number density) decreases, the distribution of the histograms broaden. For the 135 and 76 torr conditions, the histograms are skewed to lower temperatures. Average temperatures for each condition are plotted as a solid vertical line.

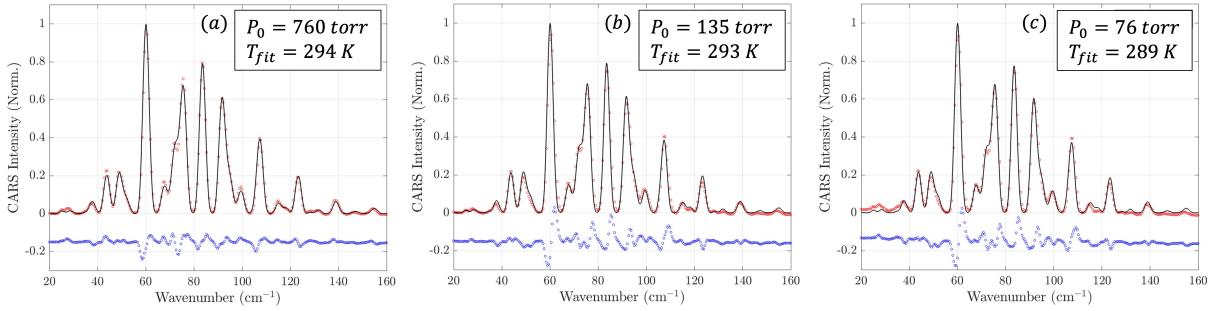

Fig. 8 Ensemble averaged temperature fits of 1000 single-shot CARS spectra of air acquired in a static cell at 296 K and a vacuum pressure of (a) 760 torr, (b) 135 torr, and (c) 76 torr. A minimal increase in noise can be seen in the residuals of the temperature fit at 135 torr and 76 torr when compared against the residuals for the temperature fit at 760 torr, as opposed to the noticeable increase in noise for the single-shot data shown in Figure 6.

fits are in good agreement with each other, as well as with the experimental plenum temperature of 296 K, denoted with a dashed red line. At 76 torr, the ensemble average temperature fit is in good agreement with the experimental plenum temperature, and the standard deviation in the single-shot data encompassed both the ensemble average and

experimental temperature. However, below 76 torr the error in temperature fit both for single-shot and ensemble averaged temperature increases significantly. This indicates that the noise in the spectra became too significant with respect to the peak CARS intensity, such that temperature could not be accurately determined. Additionally, the SNR decreases with vacuum pressure. At 76 torr, the SNR is 105. At the next lowest pressure, 42 torr, the SNR is 44 and the measurement temperature becomes more unreliable. The results for the vacuum pressures tested below 42 torr are omitted from Figure 9, as the SNR was too low to obtain a reliable temperature measurements.

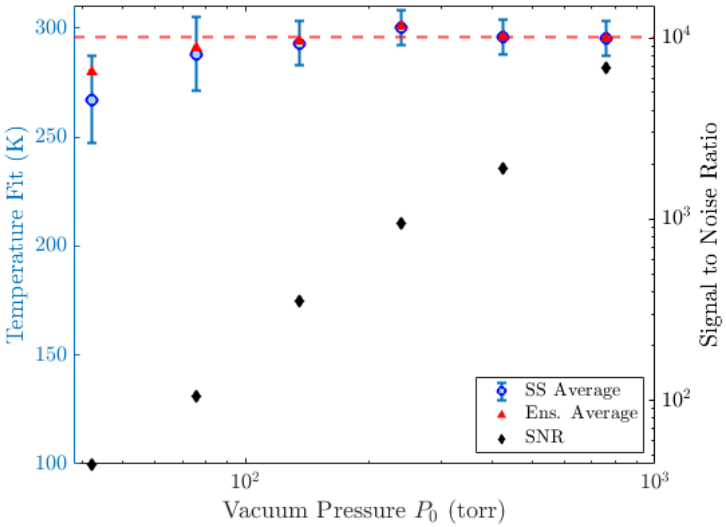

Fig. 9 Average temperature and standard deviation of measured temperature for 1000 single-shot spectra (blue circles) and ensemble average fit temperature (red triangles) compared against experimental plenum temperature (296 K, red dotted line). SNR is plotted as a function of pressure (black diamond).

B. Supersonic jet measurements

As previously discussed, CARS measurements were acquired using three supersonic nozzles with Mach numbers of 1.84, 2.64, and 3.84. The static pressure and temperature conditions for these nozzles are summarized in Table 3. Additionally, at each of the conditions tested, the translation stages were used to acquire CARS spectra at different locations across the gas jet. TS 2 was used to center the probe volume over the jet in the direction of laser propagation, which will be referred to as the x-direction. TS 1 was used to acquire CARS spectra from the center of the jet towards the side windows of the test section. TS 1 moves the probe volume perpendicular to the direction of laser propagation, which will now be referred to as the y-direction. This allows for CARS measurements to be acquired both within and outside of the pressure-matched jet. Figure 10 shows example single-shot CARS spectra for the three individual jets both within (top, a–c) and out (bottom, d–e) of the jet. The in-jet positions for the Mach 1.84, 2.64, and 3.84 nozzles were $[-6, 0]$ mm, $[-6, 0]$ mm, and $[0, 1]$ mm, respectively. The out-of-jet positions for Mach the Mach 1.84, 2.64, and 3.84 nozzles were $[-1.5, 0]$ mm, $[9, 0]$ mm, and $[0, -5]$ mm, respectively. Positions are reported as [x-coordinate, y-coordinate].

1000 single-shot spectra were recorded at locations within and outside of the jet; the average temperature and standard deviation of these individual fits are summarized in Table 4, compared against expected temperatures. The expected temperature within each jet was calculated using isentropic relations. Error in measured temperature versus expected temperature ranges from 48% for the Mach 3.84 nozzle (13 torr condition) to 15% for the Mach 2.64 nozzle. The Mach 3.84 nozzle was tested at three different conditions; at a static pressure of 13 torr the average temperature fit is 91 K and the error in measured temperature is 22%. At this condition, it is expected that the large deviation in temperature for the Mach 3.84 nozzle is mostly a result of a large probe volume with respect to the nozzle exit. As Mach number increases, nozzle exit diameter decreases. The probe volume (full-width 10%-maximum) was measured to be 0.78, 1.04, and 1.4 times larger than the exit diameters of the Mach 1.84, 2.64, and 3.84 nozzles, respectively. Thus, the probe volume is likely encompassing more ambient air for the Mach 3.84 nozzle compared to the lower

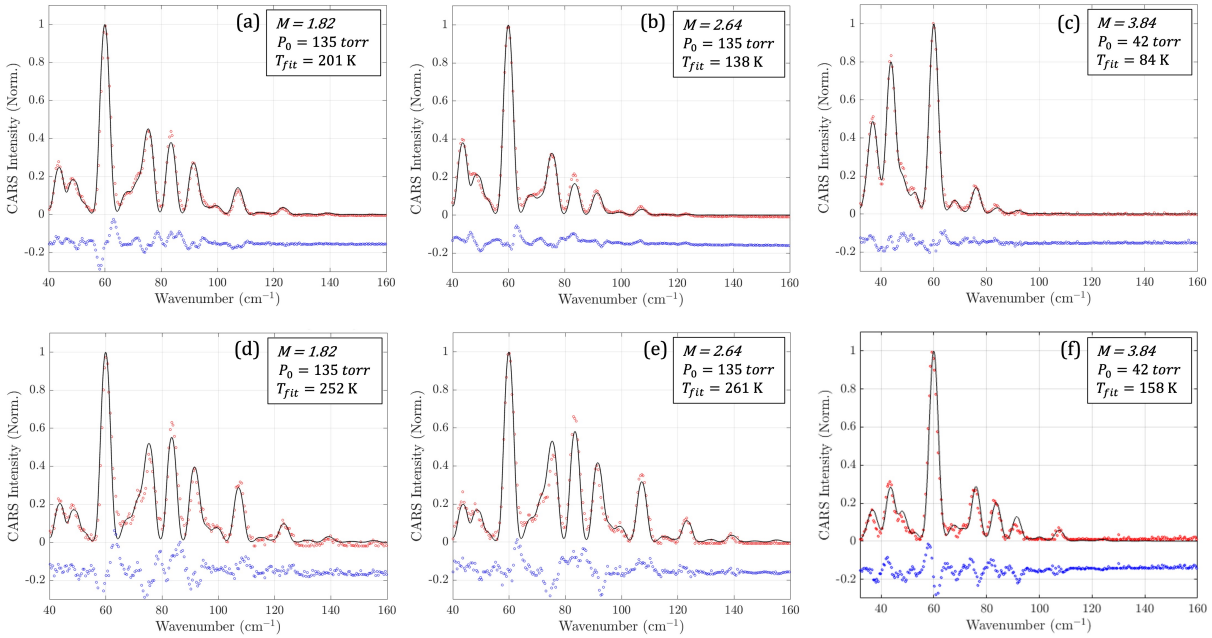

Fig. 10 Sample single-shot temperature fits for Mach 1.84, 2.64, and 3.84 nozzles (a–c) within the jet and (d–f) out of the jet.

Mach number nozzles, resulting in a higher average temperature fit. At the additional conditions of 24 torr and 13 torr, the average temperature fit is approximately 110 K, and the error in measured temperature is approximately 48%. At these conditions, the large deviation in temperature is likely due to a combination of the large probe volume as well as increased error in the fitting routine due to the decrease in number density and, consequently, SNR.

Outside of the jet, the temperature is expected to be the same as the static gas cell (296 K). For the Mach 1.84 and 2.64 nozzle, the measured temperature is closer to 250 K; this is likely a result of measuring near the unsteady jet boundary. For the Mach 3.84 nozzle at 42 torr, the measured temperature outside of the jet was significantly lower–140K. Multiple conditions were tested using the Mach 3.84 nozzle; the temperature outside of the jet is consistent across all conditions, though standard deviation does increase as number density decreases. Because the exit diameter of the Mach 3.84 nozzle is smaller than the others, the probe volume was translated a smaller distance radially from the center of the jet for these measurements. The probe volume was translated ±5 mm from the center of the Mach 3.84 nozzle, compared to ±10 mm and ±15 mm for the Mach 2.64 and Mach 1.84 nozzles, respectively. This corresponds to translating the probe volume a distance 1.5 times the Mach 3.84 nozzle diameter, versus translating a distance approximately 3 times the Mach 2.64 and Mach 1.84 nozzle diameters. The probe volume was likely not translated as far into the shear mixing layer, resulting in a lower measured temperature outside of the jet. The increase in standard deviation for the three Mach 3.84 conditions is likely a result of decreased SNR and, thus, increased error in the fitting routine as number density decreases.

1000 single-shot CARS spectra were acquired at various y-positions in the supersonic jets using TS 2; the x-position was held constant at 0 mm. Each single-shot spectrum was fit for temperature; a jet profile of temperature versus y-position was then be constructed. Figure 11 shows the compiled temperature jet profiles of the Mach 3.84 nozzle at three different static pressures; average temperature is plotted as a blue marker, and the error bars indicate standard deviation. There is good agreement in the temperature profiles across the three conditions, with a slight increase in in-jet temperature from 91 K to 109 K as static pressure decreases. This increase in temperature error can be attributed to increased error in the fitting routine as a result of decreased number density (resulting in a decrease in SNR). The decrease in number density also impacts the reliability of temperature measurements outside of the jet, as demonstrated by the relatively large standard deviation in measured temperature at the jet edges in Figure 11c. The difference in measured temperature versus the expected temperature of 74 K may be attributed to the large probe volume (7.8 mm at the full-width 10%-maximum) due to the shallow crossing angle and long focal length of the focusing lens. However, despite the large deviation from expected temperature, these results are in good agreement with the results from [20].

Table 4 Average and standard deviation measured temperature in and out of the pressure-matched jet for the three supersonic nozzles tested using the supersonic jet facility.

		In Jet			Out of Jet		
M	P_s (torr)	T_{Exp} (K)	T_{Fit} (K)	δT(%)	T_{Exp} (K)	T_{Fit} (K)	δT(%)
1.84	135	175	203 ± 2	16	296	248 ± 10	16
2.64	135	122	140 ± 1	15	296	250 ± 23	15
3.84	42	74	91 ± 1	22	296	140 ± 13	53
3.84	24	74	109 ± 2	47	296	135 ± 30	45
3.84	13	74	110 ± 3	48	296	144 ± 34	51

Based on these two experiments, the nozzle may not have a Mach number of 3.84. All y-direction scans were performed holding the x-position constant at what was believed to be the zero position. It is likely that the probe volume was not exactly centered on the jet exit in the y-direction either, resulting in an axisymmetric temperature profile. Future work will take care to mitigate this issue by translating the probe volume in a course grid and roughly fitting the spectra for temperature to ensure proper centering before data collection occurs.

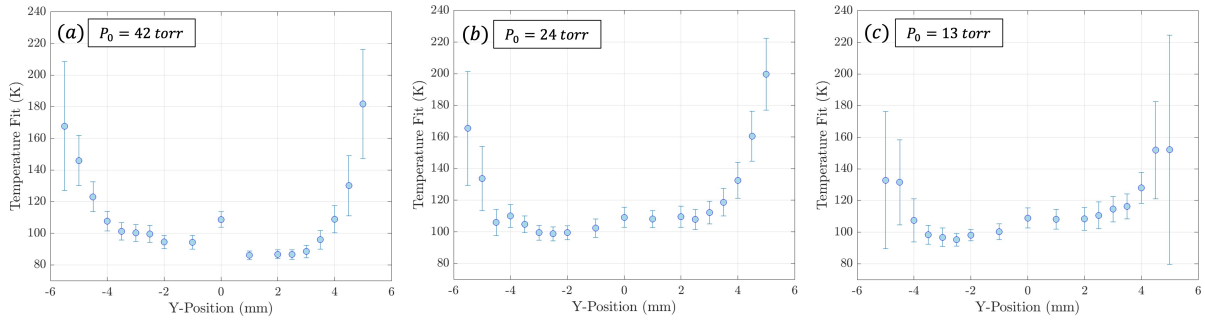

Fig. 11 Compiled temperature jet profiles for the Mach 3.84 nozzle; probe volume was translated perpendicular to the direction of laser propagation. Average temperature at each location is plotted as a marker, and standard deviation is represented by the error bars. CARS measurements were acquired at three different static pressures– (a) 42 torr, (b) 24 torr, and (c) 13 torr. The x-position was held constant at 0 mm.

C. Signal-to-noise study

A comparison of signal-to-noise ratio and temperature error as a function of gas density for both vacuum and jet data is shown in Figure 12. Only measurements at the center of each jet have been considered. The 300 to 500 wavenumber region, where no population of the Raman transitions was observed, was used to calculate noise. Additionally, CARS spectra were simulated at 50 K and 296 K and a variety of pressures; the maximum signal intensity at these conditions was normalized against the maximum signal intensity at 296 K and 760 torr and plotted in Figure 12a as a function of number density. At the same number density, the theoretical peak signal intensity is higher at 50 K compared to 296 K, due to the rotational population cluster at low wavenumber transitions which occurs at low temperatures.

As evident from Figure 12a, the SNR decreases as number density decreases. For the vacuum cell at a pressure of 42 torr ($n \approx 0.08$), SNR is approximately 45; for rotational CARS, measurement precision begins to decrease below SNR values of 60 [21]. Therefore, at number densities less than 0.08 (at 296 K) it is expected that measurement accuracy decreases. This is corroborated in Figure 12b, where error in measured temperature increases as number density decreases. A noticeable increase in fit temperature error occurs as number density decreases from 0.1 to 0.06. The number density of the three nominal test conditions for the Mach 6 tunnel summarized in Table 1 are shown in Figure 12 as dotted black lines. The number density of the three nominal test conditions for the Mach 10 tunnel summarized in Table 2 are shown in Figure 12 as dashed green lines. For certain Mach 6 conditions, the current experimental set-up would be adequate for acquiring temperature measurements. At the Mach 6 condition with a number density of 0.095,

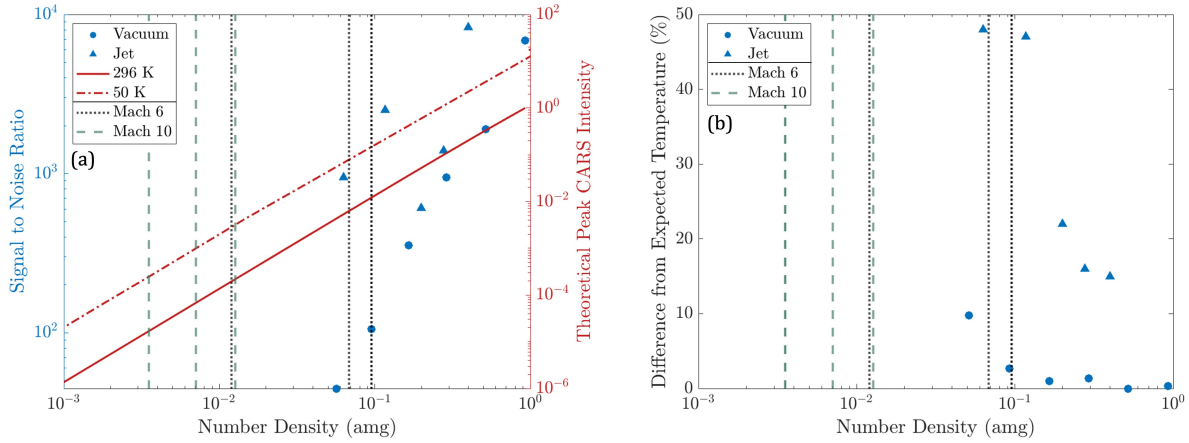

Fig. 12 (a) Signal-to-noise ratio and theoretical peak CARS intensity at 50 K and 296 K as a function of number density and (b) difference in fit temperature from expected temperature as a function of number density. Data was compiled across jet (blue triangle marker) and vacuum data (blue marker). Number densities for the three nominal Mach 6 test conditions summarized in Table 2 are plotted as three individual black dotted lines. Number densities for the three nominal Mach 10 test conditions summarized in Table 1 are plotted as three individual green dashed lines.

temperature measurements could be acquired reliably with an expected error of less than 5%. The SNR would likely be higher than the vacuum case, due to the higher expected peak intensity expected at 60 K versus 296 K. At the Mach 6 condition with a number density of 0.068, temperature measurements could likely be acquired reliably with an expected error of less than 10%. Slight modifications to the experimental set-up (i.e., adjustment in probe energy, improved beam quality at the probe volume) could potentially improve the reliability of temperature measurements at lower number densities. Given the current experimental set-up, it is likely that the peak CARS intensity, and thus the SNR, would be too low at the Mach 10 experimental number densities to collect meaningful temperature measurements in the Mach 10 wind tunnel. Future experimental modifications should be investigated using the laboratory-scale supersonic jet facility, focusing on improving SNR at these low number densities.

VI. Summary and Future Work

CARS measurements were acquired in a static gas cell at a variety of number densities, as well as in pressure-matched jets created using three different supersonic nozzles. For the static cell conditions, single shot, average, and ensemble average temperature measurements are presented. For the three nozzles, CARS measurements were acquired both in and out of the supersonic jets. Single shot spectra and average temperature measurements are presented. The capability to create temperature profiles of these supersonic jets exists, as demonstrated with the Mach 3.84 jet. Future work will focus on a more complete characterization of these supersonic nozzles, including the Mach 1.84 and 2.64 nozzles.

CARS measurements were acquired at number densities relevant to the Mach 6 and Mach 10 wind tunnels. At some conditions relevant to Mach 6, the SNR is high enough that meaningful temperature measurements can be acquired. However, an increase in temperature measurement error was observed as number density decreased, likely attributable to the decrease in signal-to-noise ratio as number density decreased. Therefore, modifications to the experimental set-up should be made to target increased CARS signal at low number densities, specifically those relevant to the Mach 10 wind tunnel. Future work will include experimental modifications and testing in the laboratory-scale supersonic jet facility, before ultimate deployment in a large scale wind tunnel. Modifications to crossing angle, probe volume, beam energies, and beam quality at the probe volume will be investigated.

Acknowledgments

The authors thank Ryan Thompson and Laurie Elkowitz from the University of Virginia Reacting Flow Laboratory for experimental assistance with the CARS system. The authors also thank W. Holt Ripley from the NASA Langley

Research Center and Amanda Braun, NASA Space Technology Graduate Research Opportunities (NSTGRO) Fellow affiliated with Purdue University, for set-up of the supersonic jet facility. N. Rodrigues and P. Danehy acknowledge the support of the NASA Space Technology Mission Directorate (STMD) Game Changing Development (GCD) project Entry Systems Modeling (ESM) and the NASA Aeronautics Research Mission Directorate (ARMD) Aerosciences Evaluation and Test Capabilities (AETC) project Test Techniques (TT). A. Stevenson was supported by a NIFS Internship at NASA Langley funded by ESM, the University of Virginia Rolls Royce Fellowship, and the National Science Foundation Graduate Research Fellowship.

References

[1] Urzay, J., "The physical characteristics of hypersonic flows," Center for Turbulence Research, Stanford University, 2020.

[2] Bathel, B. F., Johansen, C., Inman, J. A., Jones, S. B., and Danehy, P. M., "Review of Fluorescence-Based Velocimetry Techniques to Study High-Speed Compressible Flows," *51st AIAA Aerospace Sciences Meeting*, 2013. https://doi.org/10.2514/6.2013-339.

[3] Hollis, B. R., Berger, K. T., Berry, S. A., Brauckmann, G. J., Buck, G. M., DiFulvio, M., Horvath, T., Liechty, D. S., Merski, N. R., Murphy, K. J., Rufer, S. J., and Schoenenberger, M., "Entry, Descent, and Landing Aerothermodynamics: NASA Langley Experimental Capabilities and Contributions," *AIAA Scitech Forum*, 2014. https://doi.org/10.2514/6.2014-1154.

[4] Jiang, Z., Hu, Z., Wang, Y., and Han, G., "Advances in critical technologies for hypersonic and high-enthalpy wind tunnel," *Chinese Journal of Aeronautics*, Vol. 33, 2020. https://doi.org/10.1016/j.cja.2020.04.003.

[5] Schultz, D. L., and Jones, T. V., "Heat-transfer measurements in short-duration hypersonic facilities," *ADVISORY GROUP FOR AEROSPACE RESEARCH AND DEVELOPMENT NEUILLY-SUR-SEINE NEUILLY-SUR-SEINE*, 1973.

[6] Bernstein, L., and Pankhurst, R. C., "Force measurements in short-duration hypersonic facilities," *ADVISORY GROUP FOR AEROSPACE RESEARCH AND DEVELOPMENT NEUILLY-SUR-SEINE (FRANCE)*, 1975.

[7] Bonnet, J. P., Gresillon, D., and Taran, J. P., "Nonintrusive measurements for high-speed, supersonic, and hypersonic flows," *Annual Review of Fluid Mechanics*, 1998.

[8] Danehy, P. M., Wilkes, J. A., W, A. D., ad Robbins A W, J. S. B., P, P. D., and J, S. R., "Planar laser-induced fluorescence (PLIF) investigation of hypersonic flowfields in a Mach 10 wind tunnel," *25th AIAA Aerodynamics Measurement Technology and Ground Testing Conference*, 2006.

[9] Jiang, N., Hsu, P. S., Slipschenko, M., Roy, S., Lauriola, D. K., Webb, A. M., Meyer, T. R., Gragston, M., Parker, M., Portoni, P., McDermortt, C., Seitz, K., and Wadhams, T. P., "MHz Rate Flow Diagnostics in the CUBRC Mach 10 Shock Tunnel," *AIAA SciTech Forum*, 2022. https://doi.org/10.2514/6.2022-1655.

[10] Hill, L. J., Reeder, M. F., Borg, M. P., Benitez, E. K., and Running, C. L., "Implementation of Self-Aligned Focusing Schlieren for Hypersonic Boundary Layer Measurements," *AIAA SciTech Forum*, 2023. https://doi.org/10.2514/6.2023-2438.

[11] Bathel, B., Litzner, C. R., Jones, S. B., Berry, S. A., Smith, N. T., and Garbeff, T. J., "High-Speed Schlieren Analysis of Retropropulsion Jet in Mach 10 Flow," *Spacecraft and Rockets*, 2020. https://doi.org/10.2514/1.A34522.

[12] Saltzman, A. J., Beresh, S. J., Casper, K. M., Denk, B. P., Bhakta, R., De Zetter, M. E., and Spillers, R. W., "Carbon Dioxide Seeding System for Enhanced Rayleigh Scattering in Sandia's Hypersonic Wind Tunnel," *AIAA Aviation Forum*, 2022. https://doi.org/10.2514/6.2022-4131.

[13] Miles, R. B., Forkey, J. N., and Lempert, W. R., "Filtered Rayleigh Scattering Measurements in SUpersonic/Hypersonic Facilities," *AIAA 17th Aerospace Ground Testing Conference*, 1992.

[14] Danehy, P. M., O'Byrne, S., Frank, A., Houwing, P., Fox, J. S., and Smith, D. R., "Flow-Tagging Velocimetry for Hypersonic Flows Using Fluorescence of Nitric Oxide," *AIAA Journal*, Vol. 41, No. 2, 2022. https://doi.org/10.2514/2.1939.

[15] Kearney, S. P., Daniel, K. A., Wagner, J., Lynch, K. P., and Downing, C. R., "Burst-Mode Coherent Anti-Stokes Raman Scattering N_2 Thermometry in the Sandia Free-Piston Shock Tube," *AIAA SciTech Forum*, 2022. https://doi.org/10.2514/6.2022-0894.

[16] Dogariu, A., Dogariu, L., Smith, M. S., Lafferty, J., and Miles, R. B., "Single Shot Temperature Measurements using Coherent Anti-Stokes Raman Scattering in Mach 14 Flow at the Hypervelocity AEDC Tunnel 9," *AIAA SciTech Forum*, 2019. https://doi.org/10.2514/6.2019-1089.

[17] Richardson, D. R., Kearney, S. P., and Beresh, S. J., "Femtosecond Coherent Anti-Stokes Raman Spectroscopy in a Cold-Flow Hypersonic Wind Tunnel for Simultaneous Pressure and Temperature Measurements," *AIAA SciTech Forum*, 2022. https://doi.org/10.2514/6.2022-0895.

[18] Danehy, P. M., Weisberger, J., Johansen, C., Reese, D., Fahringer, T., Parziale, N. J., Dedic, C., Estevadeoral, J., and Cruden, B. A., "Non-Intrusive Measurement Techniques for Flow Characterization of Hypersonic Wind Tunnels," Tech. Rep. No. NF1676L-31725, 2018.

[19] Stauffer, H., Miller, J., Slipchenko, M., Meyer, T., Prince, B., Roy, S., and Gord, J., "Time- and frequency-dependent model of time-resolved coherent anti-Stokes Raman scattering (CARS) with a picosecond-duration probe pulse," *The Journal of Chemical Physics*, Vol. 140, 2014. https://doi.org/https://doi.org/10.1063/1.4860475.

[20] Dedic, C. E., Cutler, A. D., and Danehy, P. M., "Characterization of supersonic flows using hybrid fs/ps CARS," *AIAA Scitech Forum*, 2019. https://doi.org/10.2514/6.2019-1085.

[21] Dedic, C., "Hybrid fs/ps coherent anti-Stokes Raman scattering for multiparameter measurements of combustion and nonequilibrium," *Doctoral dissertation, Iowa State University*, 2017. https://doi.org/https://doi.org/10.31274/etd-180810-5126.

[22] Eckbreth, A., "BOXCARS: Crossed-beam phase-matched CARS generation in gases," *Applied Physics Letters*, Vol. 32, 1978. https://doi.org/https://doi.org/10.1063/1.90070.

[23] Kim, A., Dedic, C. E., and Culter, A. D., "Development of a fs/ps CARS system for temperature and species measurements in a dual-mode scramjet combustor," *AIAA Scitech Forum*, 2023. https://doi.org/10.2514/6.2023-1933.

[24] Micol, J. R., "Langley Aerothermodynamic Facilities Complex: Enhancements and Testing Capabilities," *36th AIAA Aerospace Sciences Meeting and Exhibit*, 1998.